Petrography and geochemical framework of harzburgite xenoliths of Lake Guinnadji and Ngao Djalsoka volcano from Dibi area (Adamawa plateau - Cameroon)

Abstract

Petrography and geochemical studies have been carried out on peridotite xenoliths included in pyroclastite deposits from Lake Guinnadji and Ngao Djalsoka volcano close to Dibi locality in Adamawa plateau, central Cameroon. Petrography study reveals peridotite xenoliths of protogranular and porphyroclastic textures, composed of olivine, orthopyroxene and minor amount of clinopyroxene, amphibole (?) and spinel, typical of harzburgite type. ICP-MS and ICP-OES analyses of representative samples show that they are in the range of those of the primitive mantle origin (42.4-45.0 wt.% MgO, 65.7-79.0 wt.% normative olivine). Decreased SiO_2, TiO_2, Al_2O_3, CaO contents vs MgO trends lead to a depletion from more fertile mantle by extraction of basaltic melts, leaving a refractory residue of harzburgite composition. The high REE and incompatible elements point out secondary enrichment processes which have affected peridotite xenoliths. Metasomatism caused by silicate fluids phase could be invoked. In that way, peridotites of Dibi area witness of the nature and the evolution of lithospheric mantle under the Adamawa plateau.

Keywords: Mantle xenolith, Harzburgite, Melt extraction, Metasomatism, Adamawa plateau, Cameroon

1. Introduction

The basement of African continent is composed of Archean cratons and Pan African mobile belt (Figure 1A). The Cameroon volcanic line and Adamawa plateau (Figure 1B) are among the main volcanic structures located within the Pan African belt. The studied area (Figure 1C) belongs to the central Adamawa plateau, an asymmetrical horst of mean altitude of 1100 m with 1 km difference in height vis-à-vis to its vicinity. The horst shape structure of Adamawa took place at Tertiary times after its uplift due to the rework of Pan African faults (Moreau et al., 1987) which delimit it northern and southern borders that form cliffs in the landscape. Geophysical studies carried out on Adamawa plateau have shown that Pan African faults have cut the crust down to the mantle (Dorbath et al., 1986; Nnange et al., 2000) and thus have served as natural passage for the magma to reach the surface (Moreau et al., 1987), probably after the mantle melting through adiabatic decompression process (Nkouandou et al.,

2010). The Adamawa uprising could have break up the crust-mantle equilibrium system (Njankouo Ndassa, 2020), leading to the evolution of the subcontinental mantle with the modification of its nature, structure and composition (Nkouandou et al., 2015; Njombie et al., 2018; Njankouo Ndassa, 2020). This evolution is ascertained by previous studies on mantle materials brought to the surface by Mio-Pliocene basaltic lavas flow which have shown that the nature of subcontinental mantle beneath the Adamawa plateau seems rather complex (Nkouandou et Temdjim, 2011; Nkouandou et al., 2015; Njombie et al., 2018) due to it heterogeneous composition, not yet cleared up. Recent petrological studies (Njombie et al., 2018; Njankouo Ndassa, 2020) suggest that the spinel lherzolites from Youkou (south-east of Ngaoundéré) and from the area north of Ngaoundéré have evidenced late metasomatic enrichment induced by hydrous silicate melts and that they must have experienced refertilization processes driven by the infiltration of carbonatite or carbonated silicate melts.

This present work concerns the recent collected peridotite xenoliths from Lake Guinnadji and Ngao Djalsoka volcano close to Dibi locality (35 km south of Ngaoundéré) and focuses on their geochemical feature in order to allow new insights in the nature of Adamawa mantle and its evolution processes.

2. Geological setting

Lake Guinnadji and Ngao Djalsoka are volcanic structures close to Dibi locality, which belong to the Adamawa plateau, horst of Pan African basement including 630–620 Ma pre- to syn-D1, 580–600 Ma syn-D2 and 550 Ma post-orogenic granitoids (Toteu et al, 1987, 2001; Toteu, 1990). The basement is also composed of pyroxene-and amphibole-bearing gneiss located in the south of Meiganga, showing the geochemical characteristics of Archean TTG (tonalite - trondhjemite - granodiorite), dated of Late Archean (2.6 Ga) to Palaeoproterozoic (1.7 Ga) ages with $^{207}Pb/^{206}Pb$ single-zircon evaporation method (Ganwa et al., 2008). The recent volcanic episode of Adamawa plateau, dated at 0.91 ± 0.06 Ma, yielded maars and scoria cones with associated basaltic lava flows (Temdjim et al., 2004), mainly around Ngaoundéré. At the center of Ngaoundéré area, Adamawa basement is covered by basaltic and felsic volcanic lavas of Mio-Pliocene age of 7 to 11 Ma (Gouhier et al., 1974; Temdjim et al., 2004; Nkouandou et al., 2008). At Dibi locality, hillocks of dome shape are composed exclusively of pyroclastite projections which freshness should witness of the most recent volcanic ages. The studied peridotite xenoliths have been sampled in pyroclastite projections of Dibi. Petrography and mineralogical studies carried out on Dibi lherzolite peridotites (Girod et al., 1984) sampled from the mantle by pyroclastite projections on their way to the

surface have shown that the Moho discontinuity is located at depth of 20 km, after the whole Adamawa uplift at Tertiary times.

3. Analytical Method

Studied peridotites recently discovered in pyroclastite projections of Dibi locality have undergone petrography studies using 10 thin sections prepared at the laboratory GEOPS, University Paris-Saclay, France. Modal proportions of major mineral phases (olivine, orthopyroxene, clinopyroxene and spinel, plus amphibole (?)) of studied peridotite xenoliths selected for this work have been estimated under the polarized microscope. Major element analyses have been carried out by ICP-OES (Inductively Coupled Plasma - Optical Emission Spectrometry) and trace element analyses by ICP-MS (Inductively Coupled Plasma - Mass Spectrometry) at Acme Labs of Vancouver, Canada. For the preparation of samples, about 300 mg of powder have been treated with $LiBO_2/Li_2B_4O$ flux and dissolved in HNO_3. Crucibles are fused in a furnace. The cooled bead is dissolved in ACS grade nitric acid. Loss on ignition (LOI) is determined by igniting a sample split then measuring the weight loss.

4. Results

4.1. Field work and petrography

Studied samples have been collected from pyroclastite deposits around Lake Guinnadji and Ngao Djalsoka volcano (Figure 2A) close to Dibi locality (see Table 1 for sample coordinates). Ngao Djalsoka belongs to the volcanic cones of ENE trend (Figure 1C). As many volcanoes of the area, Ngao Djalsoka is composed of various type of pyroclastite projections including welded tuffs (including blocks of 5-20 cm in size), bombs 10-30 cm in size, rare blocks 30-60 cm in size, with some showing porous structure, lapillis, volcanic ashes, and in addition some roped lavas. Pyroclastic projections around Lake Guinnadji and Ngao Djalsoka volcano have the same mineral composition: yellowish or bluish olivine crystals, blackish pyroxene crystals and tiny sparkling plagioclase microliths.

Studied peridotite xenoliths have been found in such basaltic blocs (Figure 2). They exhibit yellowish (Figure 2B) or blackish colour (Figure 2C). They are sub-rounded or sub-angular in shape and show sharp contact with basaltic host lava (Figure 2D). The main distinguished minerals of peridotite xenoliths are blue yellowish olivine crystals (60 to 70 volume %) and undistinguished blackish ones (pyroxene, amphibole or spinel?). Whitish crumbly fragments (5 to 7 cm) of crustal origin are packed up in the matrix. The contact between crustal enclave and basaltic host lava show a thin brown corona.

Under plane polarized light (Figure 3), Lake Guinnadji and Djalsoka volcano xenoliths exhibit protogranular (Figure 3A and B) or porphyroclastite texture (Figure 3C and D), following the nomenclature of Mercier and Nicolas (1975). All selected samples are mainly composed of olivine, orthopyroxene, clinopyroxene, amphibole (?) and ± spinel. Large crystals are outlined by dots in the borders.

Olivine crystals (4 to 6 mm) are the most abundant component (74-86 %, Table 2). The aggregates of small (< 1mm) recrystallized olivine crystals show mosaic-shaped with straight-lined boundaries. Few (2-8 %) clinopyroxene crystals (1 to 2 mm) occur in all samples specially in contact with remnant orthopyroxene crystals. Orthopyroxene crystals (10-17 %) are 2 to 4 mm size. Large orthopyroxene crystals are mostly remnant and closely link to olivine crystals. All the samples show recrystallization signs marked by the occurrence of two kinds of olivine and enstatite crystals: large elongated and undulated grains (Figures 3A and D) and small generally polygonal strain ones (Figures 3B and C). Spinel (1-2 %) are up to 1 mm in size. They always show vermicular shape and frequently occur between pyroxene crystals. Some spinels show dot shape feature. Scarce amphibole (?) (2 to 3 min in size, 0-1 %) crystals occur in some samples (Figure 3A). They are ovoid in shape are show small dots in their borders. Estimated volume percentages of mineral phases (Table 2) plot in the field of harzburgite in ternary diagram (Figure 4) of Le Maitre (2002).

4.2. Geochemical features

Geochemical composition of some xenoliths from surroundings of Lake Guinnadji and Djalsoka volcano are listed in Table 3. Major elements contents show variable values. SiO_2 are between 40.59 and 43.60 wt.%. TiO_2 contents are relatively low (< 0.21 wt.%), samples HD1 and HD3 exhibit the lowest TiO_2 values (0.07-0.06 wt.%). Al_2O_3 contents witness of two groups, low content (0.62-0.71 wt.% for samples HD1, HD3, HD5 and MO-03) and relatively high content (1.23-1.54 wt.% for samples HD2, MO-10 and MO-12). Note that CaO contents vary in the same way as Al_2O_3. Highest amount of Al_2O_3 and CaO correspond to higher amount of modal clinopyroxene (5-8 against 2-5 vol.% in the other group, see Table 2). These variations lead to relatively constant CaO/Al_2O_3 ratios for all samples, between 0.68 and 0.97, with the mean value close to the Primitive upper mantle values (0.80, McDonough and Sun, 1995). Al_2O_3/TiO_2 ratios vary between 4.47 and 11.00.

Fe_2O_3 contents are relatively constant (10.6-15.2 wt.%). MnO contents are low and constant (0.14-0.17 wt.%). MgO contents are high with some variations, leading to

contrasting Mg# (=100*(MgO/40.304) / ((MgO/40.304) + (FeOt/71.844)) between 85.0 and 88.8.

Alkali contents Na_2O (0.08-0.26 wt.%) and K_2O (0.05-0.13 wt.%) are low. Na_2O/Al_2O_3 ratios lay between 0.13 and 0.27, compared to 0.11 value of sub continental mantle (McDonough, 1990). P_2O_5 contents are low (0.03-0.07 wt.%).

SiO_2, $A1_2O_3$, CaO, Na_2O and TiO_2 contents of studied xenoliths have been plotted against their MgO content (Figure 5). All Harker diagrams show rather negative trends with increasing MgO values.

CIPW normative analyses (Tale 3) confirm petrographical observations. Normative olivine (65.7-81.8 wt.%) is strongly dominant. Normative hypersthene (9.4-21.2 wt.%) is in higher amount than normative diopside (0.2-3.1 wt.%), that is typical of harburgites.

First transitional elements (Sc, V, Ni, Co and Cr) of analysed samples vary widely (see Table 3). Sc contents (7-9 ppm) are low, Ni (2111-2356 ppm), Cr_2O_3 (0.03-0.31 wt.%) and Co (119-169 ppm) contents are high, while V vary between 15-and 53 ppm. Incompatible trace elements contents are low and show wide variation: Rb: 0.8-4.3 ppm, Sr: 14.5-85.5ppm, Ba: 8-60 ppm, Cs: 0.01-0.1 ppm and Th: 0.1-0.74 ppm. Zr: 5.6-29 ppm and Hf: 0.1-0.6 ppm give relatively constant Zr/Hf ratios of 36-56. Nb and Ta contents are also low and give contrasted Nb/Ta ratios (4.3-41) while Nb/Th ratios (8-16) are rather high. Y (0.6-2.6 ppm) and Ho (0.02-0.1 ppm) give Y/Ho ratios of 20-40. Sr/Nd ratios of studied peridotites (11.1-15.8) are close to mantle peridotite (Jochum et al., 1989).

Normalized REE ratios of studied xenoliths are shown in Figure 6A. Samples display large variations in REE distribution patterns. Overall, the xenoliths are strongly enriched in LREE (LaN/SmN = 3.2-13.5). Moreover, LaN/YbN ratios range between 11.42 and 23.25. Normalized La are up to 10 times the mantle values, especially for samples of MO group which are characterized by relatively high REE values compared to samples of HD group (Table 3 and Figure 6A).

In spider diagram (Figure 6B), normalized trace elements display rather regular decrease values from U to Lu. Samples of MO group are characterized by negative anomalies in K, Ti and also in P. Compared with samples of MO group, HD group samples display negative anomalies in Ta and positive anomalies in Cs except HD5. All samples exhibit positive anomalies in Zr and most of them for U except MO-10 and MO-12.

5. Discussion

Geophysical studies carried out on Adamawa plateau (Dorbath et al., 1986; Poudjom Djomani et al., 1992, 1995; Nnange et al., 2000, 2001) have evidenced the rework of Pan African faults which have crosscut the Adamawa basement and reach the underlined lithospheric mantle, serving as pathways for the ascending magmas (Moreau et al., 1987). Studied xenoliths should have been sampled in such conditions, probably during transpressive actions of those faults or after upwelling. It has previously been shown, according to lherzolite xenoliths equilibria, that the Moho discontinuity is shallow, 20 km beneath the Dibi locality (Girod et al., 1984; Dautria and Girod, 1986.) due to the whole Adamawa uplift after the rework of Pan African faults (Moreau et al., 1987), leading to the compositional evolution of Adamawa sub continental mantle (Njankouo Ndassa, 2020).

Petrography and geochemical features of peridotite xenoliths sampled around Lake Guinnadji and Ngao Djalsoka volcano witness of the complex nature of sub-continental mantle beneath Dibi volcanic area. Field work data show that peridotite xenoliths occurs mainly in pyroclastites projections exhibiting porous structure. Their sub-rounded or sub-angular shape may reflect the different sample depths within the mantle. Modal and normative analyses (Tables 2 and 3) point out far higher amount of orthopyroxene vs. clinopyroxene, typical of harzburgite type.

Geochemical data show some variation ranges of major and trace elements (Table 3, Figure 5), certainly linked with the compositional diversity of the underlined mantle or processes because of its evolution. It is clear that geochemical analyses of studied harzburgite xenoliths characterize materials originate from a depressed mantle. MgO contents (42.4- 45.0 wt.% for Mg# (85.0-88.8) are close to typical harzburgite mantle (45-47 wt.% MgO for Mg# > 85, Maaløe and Aoki, 1977; McDonough, 1990). As comparison, Youkou lherzolite presents a higher Mg# ratio of 90.0 for a lower MgO content of 40.0 wt.% (Table 3).

Studied xenoliths exhibit protogranular and porphyroclastite textures which are diagnostic for mantle peridotites (Mercier and Nicolas, 1975). Remnants and recrystallized features of crystal phases may be interpreted as tectonic markers of their evolutionary setting.

Low contents of incompatible elements and their ratios (Zr/Hf, Nb/Ta, Y/Ho, Sc/Nd are arguments in favour of mantle materials origin (McDonough and Sun, 1995) of Lake Guinnadji and Ngao Djalsoka volcano peridotites instead of upper mantle fractional crystallization cumulates. Cumulate origin of studied xenoliths is excluded if one considers the fact that all xenoliths exhibit an overall depletion in the HREE, resulting in higher

LaN/YbN ratios (11.5-23.3) similar to those of fertile peridotite xenoliths worldwide (McDonough, 1990).

K_2O vs MgO diagram (Figure 7) is used to discriminate xenoliths of cumulate origin from those of off-craton or cratonic origins (after Downes et al., 2004; see discussions in Lee et al., 2000; Downes, 2001). It is clear according to this diagram that studied xenoliths are residual peridotites of off-craton origin. According to La vs Yb diagram (Figure 8), all xenolith samples fall almost within the field of subcontinental harzburgite composition.

Studied xenoliths exhibit low values of CaO/MgO ratios (0.01-0.03), close to those of residual harzburgite peridotites (CaO/MgO < 0.02; Lenoir et al., 2001) and relatively high MgO contents (42.4-45.0 wt.%) compared to samples which have not experienced excessive loss of a basaltic component with ≤ 40.5-41.0 wt.% MgO (Maaløe and Aoki, 1977; McDonough and Sun, 1995). REE data with strong LREE enrichment and LREE/HREE fractionation of the bulk-rocks distinguish Lake Guinnadji and Ngao Djalsoka peridotites as metasomatized harzburgites as proposed by Downes (2001) for ultramafic xenoliths from Western and Central Europe.

Mg# vs CaO (wt.%) diagram (Figure 9) and very high LaN/YbN ratios show that Lake Guinnadji and Ngao Djalsoka peridotites have undergone rather high partial melting degree, between 20 and 30 % (Figure 9) and have been modified by secondary enrichment process (McDonough and Sun, 1995). It is also worth mentioning that the contrast geochemical signatures of the whole–rock of the studied peridotites (Figure 5) cannot be attributed to melt depletion or only partial melting processes, therefore the observed enrichments of LREE and incompatible elements strongly reflect the effect of subsequent metasomatism of the Lake Guinnadji and Ngao Djalsoka volcano peridotites (Meshesha et al., 2014). The occurrence of hydrous phase (amphibole?), suggested in the studied xenoliths, is known in upper mantle (Dawson and Smith, 1982). Spiderdiagrams of Figure 6 show variable enrichment of incompatible elements especially positive anomalies in U and negative anomalies in Ta leading to variable degrees of cryptic metasomatism (Mesheshia et al., 2014). Subcontinental mantle under Dibi locality may have evolved through two mantle processes: (1) varying degrees of depletion of a fertile mantle by extraction of basaltic melts, leaving a refractory residue, in view of the systematic negative trends of CaO, SiO_2, Al_2O_3, TiO_2 and Na_2O and (2) modal metasomatism superimposed on cryptic type. Silicate fluids phase are behind the cryptic type metasomatism, according to relatively high ratios of Na_2O/Al_2O_3 (0.13-0.27) more than 0.11 of primitive mantle (McDonough, 1990), relative to carbonate type as CaO/Al_2O_3 ratios of analysed samples are closed to primitive mantle values (0.80). Moreover,

high Zr/Hf (=36-56) and Nb/Ta (=4.3-225.7) which vary wildly relative to mantle values (Zr/Hf=36.30 and Nb/Ta= 17.5, Sun and McDonough, 1989), are interpreted as the result of pervasive silica melt-solid interaction with significant amounts of trapped melt and sample MO-03 with low Nb/Ta (4.3) would have interact with a limited amount of trapped melt (Niu, 2004).

Conclusion

Petrography and geochemistry preliminary data carry out on Lake Guinnadji and Ngao Djalsoka volcano peridotites determine the xenolith of mantle origin exhibiting protogranular and porphyroclastic textures. Mineral are olivine, orthopyroxene and minor amount of clinopyroxene, spinel, plus amphibole (?). Studied xenoliths are harzburgite type peridotites which have undergone high partial melting degree, between 20 and 30 % and have been modified by secondary enrichment process. Subcontinental mantle under Dibi locality have evolved through varying degrees of depletion of a more fertile mantle by extraction of basaltic melts and modal metasomatism superimposed on cryptic type.

References

Balashov Y.A., 2009. Development of a heterogeneity in the lithosphere: Geochemical evidence. Petrology 17, 1, 90-100.

Dautria, J.M., Girod, M., 1986. Les enclaves de lherzolite à spinelle et plagioclase du volcan de Dibi (Adamaoua, Cameroun): des témoins d'un manteau supérieur anormal. Bulletin de Minéralogie 109, 3, 275-286.

Dawson J.B., Smith J.V., 1982. Upper-mantle amphiboles: a review. Mineralogical Magazine 45, 35-46.

Dorbath C., Dorbath L., Fairhead J.D., Stuart G.W., 1986. A teleseismic delay time study across the Central African Shear Zone in the Adamawa region of Cameroon, West Africa. Geophysical Journal of the Royal Astronomical Society 86, 751-766.

Downes H0, 2001. Formation and modification of the shallow sub-continental lithospheric mantle: a review of geochemical evidence from ultramafic xenolith suites and tectonically emplaced ultramafic massifs of western and central Europe. Journal of Petrology 42, 1, 233-250.

Downes H., Macdonald R., Upton B.G.J., Cox K.G., Bodinier J.L, Mason, P.R.D., James D., Hill P.G, Hearn Jr C., 2004. Ultramafic xenoliths from the Bearpaw Mountains,

Montana, USA: Evidence for multiple metasomatic events in the lithospheric mantle beneath the Wyoming Craton. Journal of Petrology 45, 8, 1631-1662.

Friedman E., Polat A., Thorkelson D.J., Frei, R., 2016. Lithospheric mantle xenoliths sampled by melts from upwelling asthenosphere: The Quaternary Tasse alkaline basalts of southeastern British Columbia, Canada. Gondwana Research 33, 209-230.

Ganwa A.A., Frisch W., Siebel W., Ekodeck G.E., Cosmas S.K., Ngako V., 2008. Archean inheritances in the pyroxene-amphibole bearing gneiss of the Méiganga area (Central North Cameroon): Geochemical and 207Pb/206Pb age imprints. Comptes Rendus Géoscience 340, 211-222.

Girod M., Dautria J.M., Ball E., Soba D. 1984. Estimation de la profondeur du Moho, sous le massif volcanique de l'Adamaoua (Cameroun), à partir de l'étude d'enclaves de lherzolite. Comptes Rendus de l'Académie des Sciences, Paris 298, II,16, 699-704.

Gouhier J., Nougier J., Nougier D., 1974. Contribution à l'étude volcanologique du Cameroun ('Ligne du Cameroun', Adamaoua), Annales de la Faculté des Sciences de l'Université de Yaoundé, Cameroun 17, 3-48.

Hofmann A.W., 1988. Chemical differentiation of the Earth: The relationship between mantle, continental crust, and oceanic crust. Earth and Planetary Science Letters 90, 297-314.

Ishii T., Robinson P.T., Maekawa H., Fiske R., 1992. Petrological studies of peridotites from diapiric serpentinite seamounts in the Izu-Ogasawara-Mariana Forearc, Leg 125. Proceeding of the Ocean Drilling Program, Scientific Results 125, 445-485.

Jochum K.P., McDonough W.F., Palme H., Spettel B., 1989. Compositional constraints on the continental lithospheric mantle from trace elements in the spinel peridotite xenolith. Nature 340, 548-550.

Lee C.T., Rudnick R.L., McDonough W.F., Horn I., 2000. Petrologic and geochemical investigation of carbonates in peridotite xenoliths from northeastern Tanzania. Contributions to Mineralogy and Petrology 139, 470-484.

Le Maitre R.W. (Ed.), 2002. Igneous Rocks, A Classification and Glossary of Terms. (Recommendations of the IUGS Subcommission on the Systematics of Igneous Rocks). Cambridge University Press, Cambridge, 252 p.

Lenoir X., Garrido C.G., Bodinier J.L., Dautria J.M., Gervilla F., 2001. The recrystallization front of the Ronda peridotite: Evidence for melting and thermal erosion of subcontinental lithospheric mantle beneath the Alboran Basin. Journal of Petrology 42, 141-158.

Maaløe S., Aoki K., 1977. The major element composition of the upper mantle estimated from the composition of lherzolites, Contributions to Mineralogy and Petrology 63, 161-173.

McDonough W. F., Sun S.S., 1995. “The Composition of the Earth”, Chemical Geology 120, 223-253.

McDonough W.F., 1990. Constraints on the composition of the continental lithospheric mantle. Earth and Planetary Science Letters, 101, 1-18.

Mercier J.C.C., Nicolas A., 1975. Textures and fabrics of upper-mantle peridotites as illustrated by xenoliths from basalts. Journal of Petrology 16, 2, 454-487.

Meshesha D., Shinjo R., Orihashi Y., 2014. Geochemical and Sr–Nd–Pb isotopic compositions of lithospheric mantle: Spinel lherzolites in alkaline basalts from the northwestern Ethiopian plateau. Journal of Mineralogical and Petrological Sciences 109, 241-257.

Moreau C., Regnoult J.M., Déruelle B., Bobineau B., 1987. A new tectonic model for Cameroon line, central Africa. Tectonophysics 139, 317-334.

Niu Y., 2004. Bulk-rock major and trace element compositions of abyssal peridotites: Implications for mantle melting, melt extraction and post-melting processes beneath Mid-Ocean Ridges. Journal of Petrology 45, 12, 2423-2458.

Njankouo Ndassa Z.N., 2020. Pétrologie et géochimie des péridotites mantelliques en enclaves dans les basaltes au nord de Ngaoundéré: nature du manteau subcontinental du plateau de l’Adamaoua (Plateau de l’Adamaoua, Cameroun, Afrique centrale). Thèse de l’Université de Ngaoundéré, Cameroun 232 pp +annexe.

Njombie M.P.W., Temdjim R., Foley S.F., 2018. Petrology of spinel lherzolite xenoliths from Youkou volcano, Adamawa Massif, Cameroon Volcanic Line: mineralogical and geochemical fingerprints of sub-rift mantle processes. Contributions to Mineralogy and Petrology 173, 13.

Nkouandou O.F., Bardintzeff J.M., Fagny A.M., 2015. Sub-continental lithospheric mantle structure beneath the Adamawa plateau inferred from the petrology of ultramafic xenoliths from Ngaoundéré (Adamawa plateau, Cameroon, Central Africa). Journal of African Earth Sciences 111, 26-40.

Nkouandou O.F., Ngounouno I., Déruelle B., 2010. Géochimie des laves basaltiques récentes des zones Nord et Est de Ngaoundéré (Plateau de l’Adamaoua, Cameroun, Afrique Centrale): pétrogenèse et nature de la source. International Journal of Biological and Chemical Sciences 4, 4, 984-1003.

Nkouandou O.F., Ngounouno I., Déruelle B., Ohnenstetter D., Montigny R., Demaiffe D., 2008. Petrology of the Mio-Pliocene Volcanism to the North and East of Ngaoundéré (Adamawa-Cameroon). Comptes Rendus Géoscience 340, 27-38.

Nkouandou O.F., Temdjim R., 2011. Petrology of spinel lherzolite xenoliths and host basaltic lava from Ngao Voglar volcano, Adamawa Massif (Cameroon Volcanic Line, West Africa): equilibrium conditions and mantle characteristics. Journal of Geosciences 56, 375-387.

Nnange J.M., Ngako V., Fairhead J.D., Ebinger C.J., 2000. Depths to density discontinuities beneath the Adamawa Plateau region, Central Africa, from spectral analyses of new and existing gravity data. Journal of African Earth Sciences 30, 4, 887-901.

Nnange J.M., Poudjom Djomani Y.H., Fairhead J.D., Ebinger C., 2001. Determination of the isostatic compensation mechanism of the region of the Adamawa dome, West Central Africa using the admittance technique of gravity data. African Journal of Science and Technology 1, 4, 29-35.

Poudjom Djomani Y.H., Diament M., Albouy Y., 1992. Mechanical behavior of the lithosphere Beneath the Adamawa Up lift (Cameroon, West Africa) based on gravity data. Journal of African Earth Sciences 15, 81-90.

Poudjom Djomani Y.H., Nnange J.M., Diament M., Ebinger C.J., Fairhead J.D., 1995. Effective elastic thickness and crustal thickness variation in west central Africa inferred from gravity data. Journal of Geophysical. Research 100, 22047-22070.

Sun, S.-S., McDonough, W.F., 1989. Chemical and isotopic systematics in ocean basalt: implications for mantle composition and processes. In: Saunders, A. D. & Norry, M. J. (Eds.) Magmatism in the Ocean Basins. Geological Society, London, Special Publications 42, 313-345.

Tamen J., Nkoumbou C., Reusser E., Tchoua F., 2015. Petrology and geochemistry of mantle xenoliths from the Kapsiki Plateau (Cameroon Volcanic Line): Implications for lithospheric upwelling. Journal of African Earth Sciences 101, 119-134.

Temdjim, R., Boivin, P., Chazot, G., Robin, C., Rouleau, E., 2004. L'hétérogénéité du manteau supérieur à l'aplomb du volcan de Nyos (Cameroun) révélée par les enclaves ultrabasiques. Comptes Rendus Géoscience 336, 1239-1244.

Toteu S.F., 1990. Geochemical characterization of the main petrographical and structural units of Northern Cameroon: implications for Pan-African evolution. Journal of African Earth Sciences 10, 4, 615-624.

Toteu S.F., Michard A., Bertrand J.M., Rocci G., 1987. U/Pb dating of Precambrian rocks from northern Cameroon, orogenic evolution and chronology of the Pan-African belt of Central Africa. Precambrian Research 37, 1, 71-87.

Toteu S.F., Van Schmus W.R., Penaye J., Michard A., 2001. New U-Pb and Sm-Nd data from north-central Cameroon and its bearing on the pre-Pan African history of central Africa. Precambrian Research 108, 1-2, 45-73.

Table captions

Table 1. Coordinates of Lake Guinnadji and Ngao Djalsoka volcano peridotite xenoliths.

Table 2. Modal estimation of compositional phases of studied peridotite xenoliths.

Table 3. ICP-MS and ICP-AES of whole rock major and trace elements analyses of Lake Guinnadji and Ngao Djalsoka volcano harzburgites; note that LOI are negative as all Fe is calculated as Fe_2O_3. CIPW normative analyses. Youkou lherzolite analysis (Njombie et al., 2018) added for comparison.

Figure captions

Figure 1. A: Main African cratons, B: Cameroon volcanic line and Adamawa plateau volcanic area, C: Location of studied area of Guinnadji Lake and Djalsoka volcano.

Figure 2. A: Panoramic view of north hillside of Djalsoka volcano, B: Sub-angular, C: Sub-rounded, and D: Rounded shape of studied peridotite xenoliths.

Figure 3. Photomicrographs of Lake Guinnadji and Ngao Djalsoka xenolith textures. A and B: Protogralular, C and D: Porphyroclastic textures. Scale bar represents 1 mm. amph = amphibole, cpx = clinopyroxene, opx = orthopyroxene, spl = spinel.

Figure 4. Nomenclature of studied peridotite xenoliths according to the classification scheme of Le Maitre (2002). Dibi (this study): Lake Guinnadji (square) and Ngao Djalsoka volcano (triangle). Data from Youkou, Kapsiki plateau and Ngao Voglar are added for comparison.

Figure 5. Major elements contents vs MgO content Harker diagrams of Lake Guinnadji and Ngao Djalsoka volcano xenoliths.

Figure 6. Chondrite normalized REE (a) and primitive mantle normalized trace elements (b) abundances of the studied peridotite xenoliths according to McDonough and Sun (1995).

Figure 7. K_2O vs MgO diagram for studied xenoliths. Field of off-craton and cratonic mantle spinel peridotites from Downes et al. (2004). Analyses out of these fields correspond to cumulates. Lake Guinnadji (square), Ngao Djalsoka volcano (triangle), Youkou (circle),

Figure 8. Peridotite xenoliths from Ngao Djalsoka and Lake Guinnadji plotted in La vs Yb diagram after Balashov (2009). Youkou lherzolite (Njombie et al., 2018) is plotted for comparison. BSE = Bulk Silicate Earth "pyrolite", DM-EM line = Depleted Mantle - Enriched Mantle. Same symbol as Figure 9.

Figure 9. Mg# vs CaO (wt.%) diagram for Lake Guinnadji and Ngao Djalsoka peridotites. Same symbols as Figure 8. Percentage of partial melting from a primitive source is indicated by the line at the top (from Friedman et al., 2016). Added for comparison: Youkou lherzolite (circle, Njombie et al., 2018), Torishima and Conical Seamount: the dark gray shaded region represents harzburgite data, and the light grey shaded region represents dunite data (from Ishii et al., 1992).

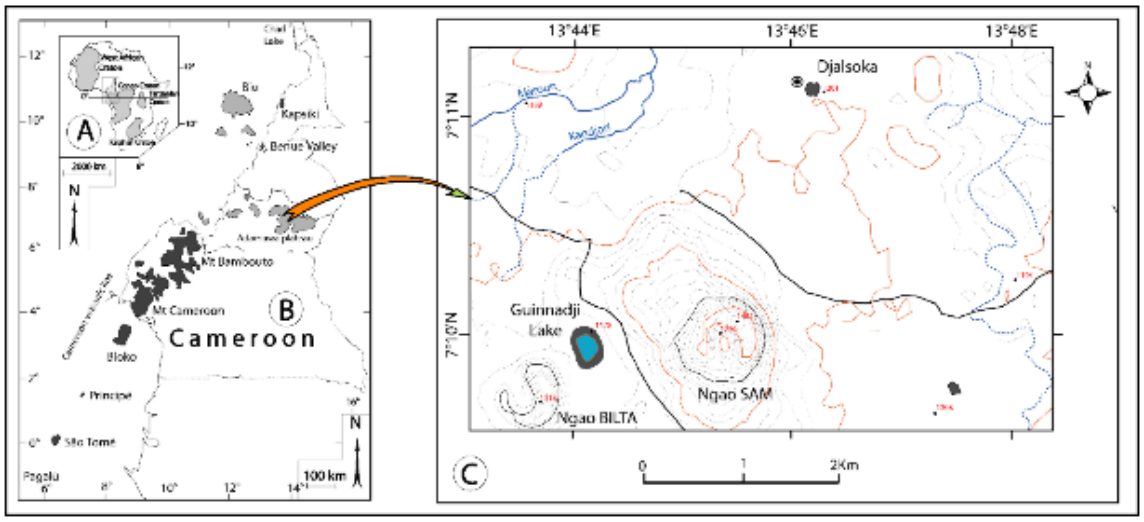

Figure 1

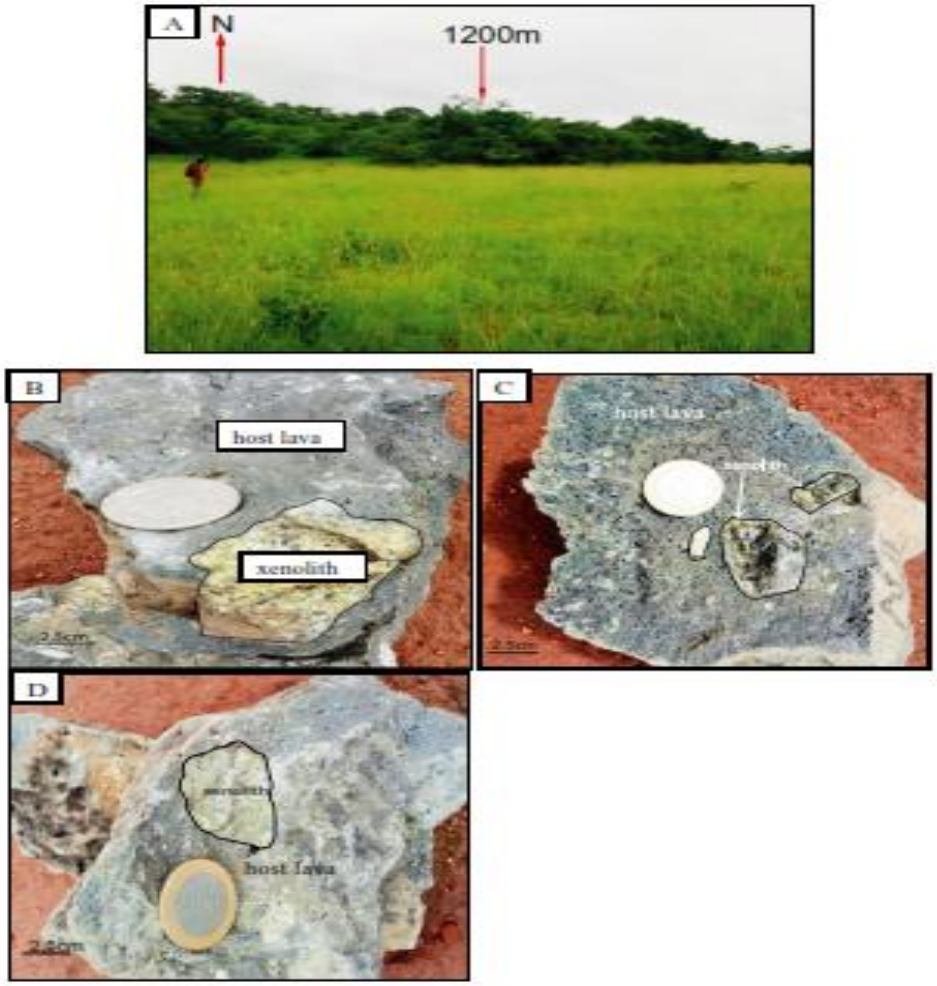

Figure 2

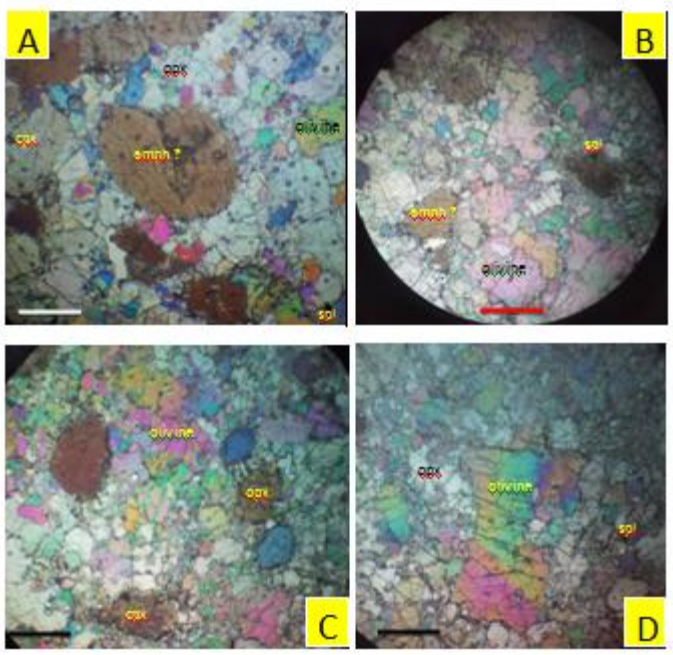

Fig 3

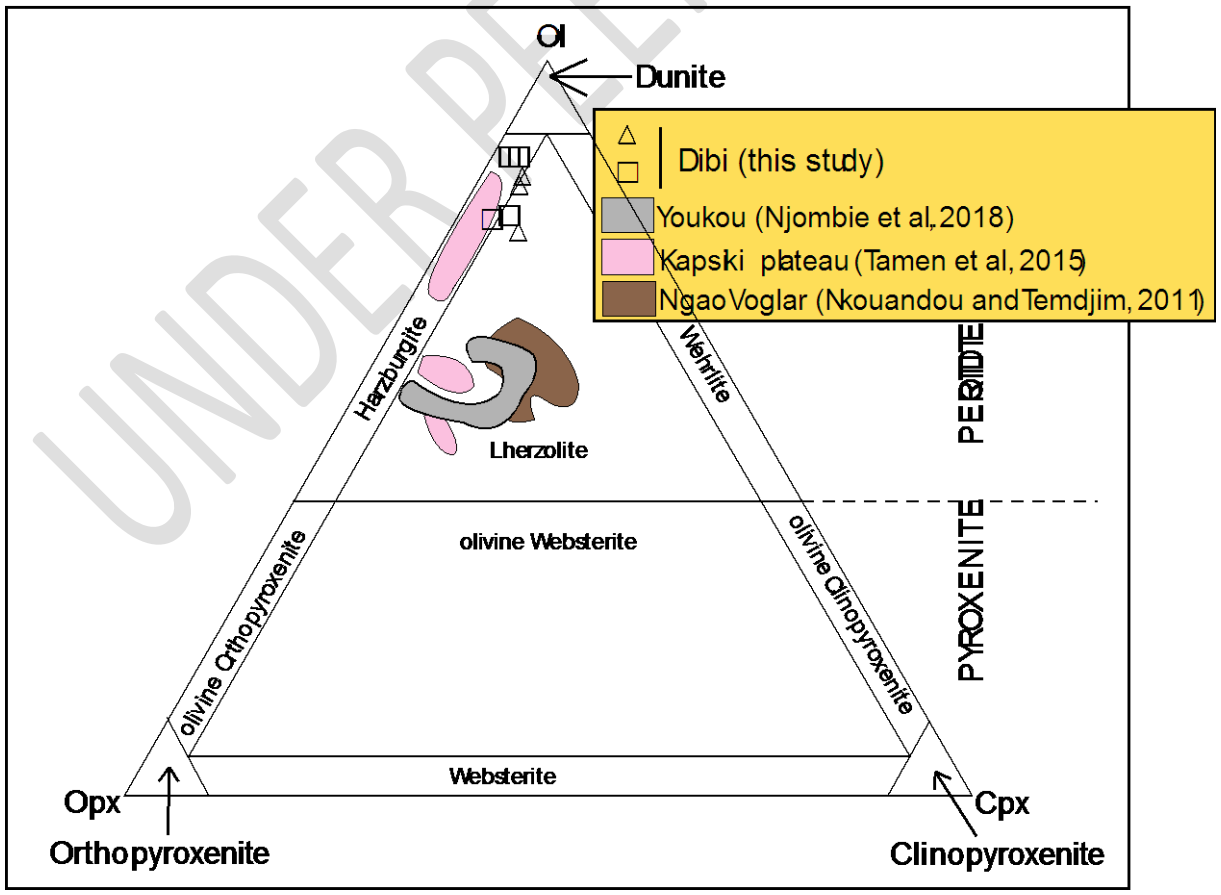

Fig 4

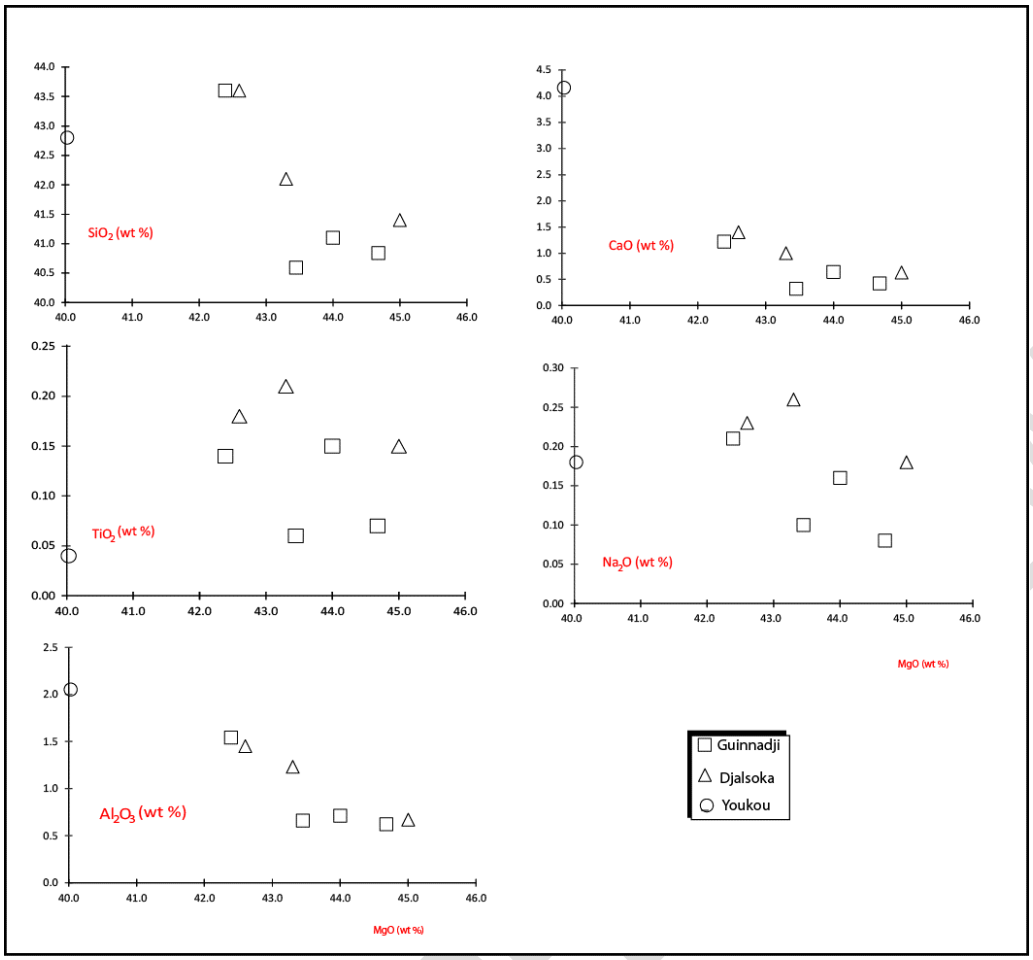

Fig 5

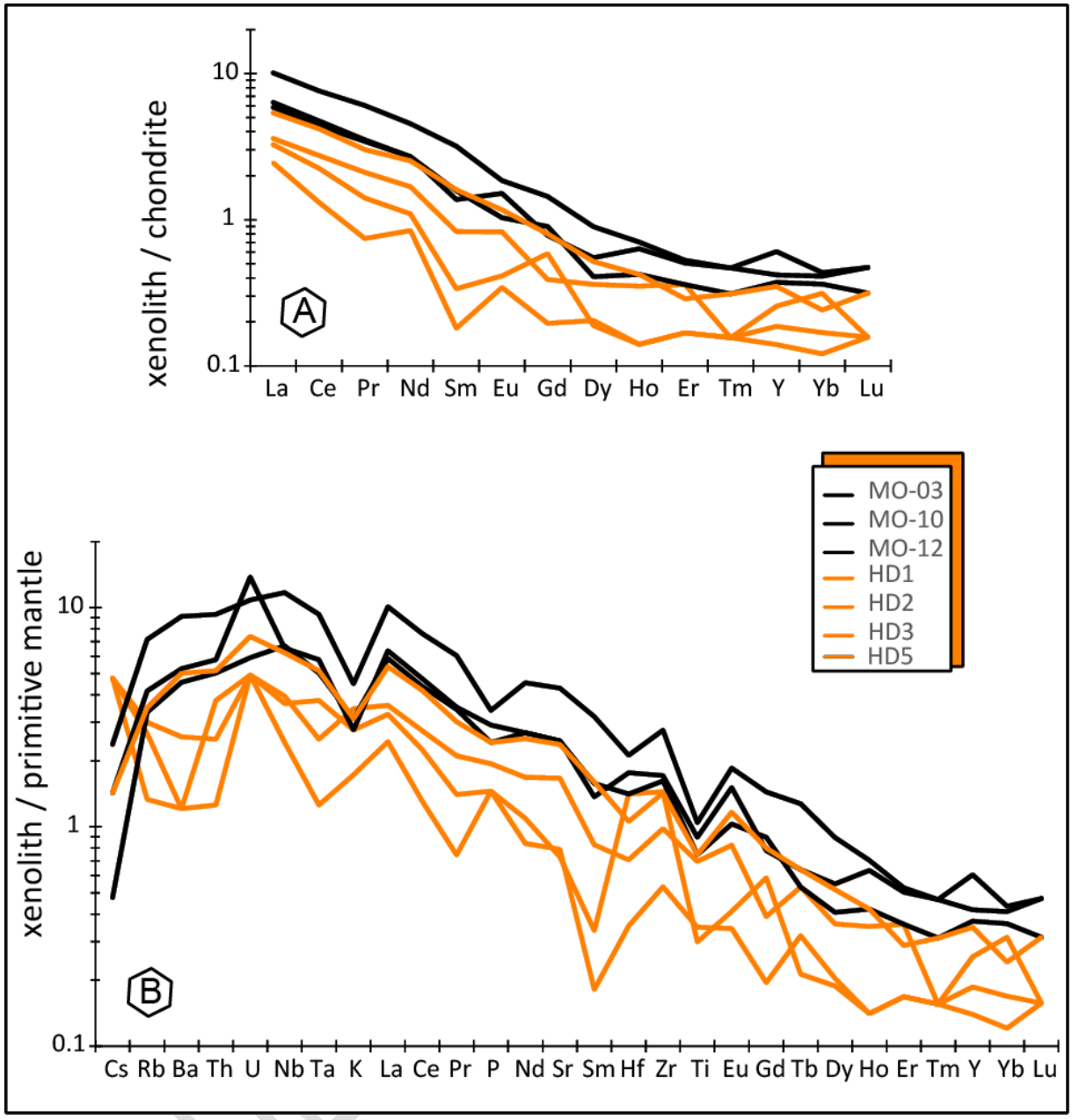
xenolith / chondrite
10
1
0.1
A
La Ce Pr Nd Sm Eu Gd Dy Ho Er Tm Y Yb Lu
MO-03
MO-10
MO-12
HD1
HD2
HD3
HD5
xenolith / primitive mantle
10
1
0.1
B
Cs Rb Ba Th U Nb Ta K La Ce Pr P Nd Sr Sm Hf Zr Ti Eu Gd Tb Dy Ho Er Tm Y Yb Lu

Fig 6

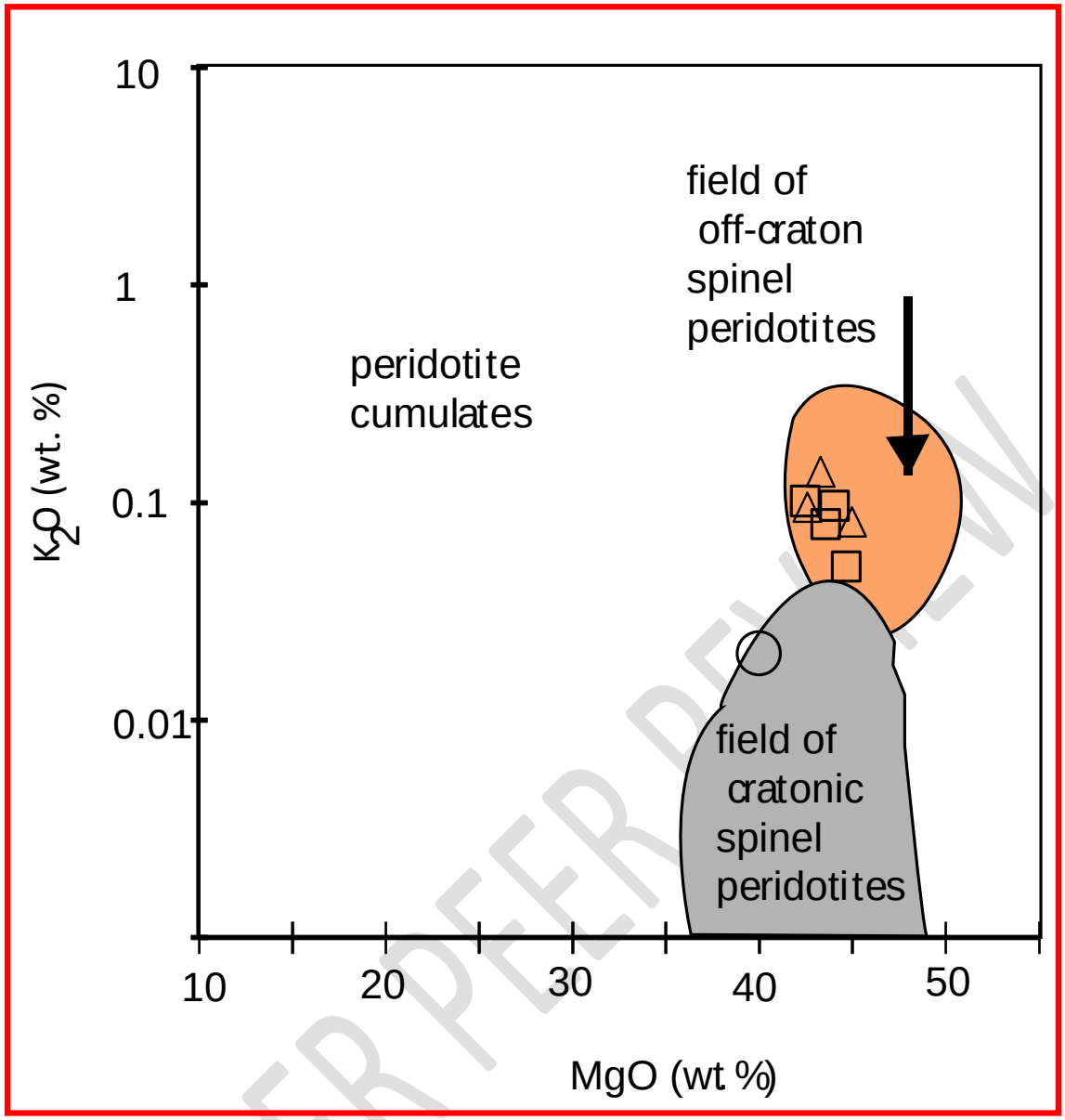

Fig 7

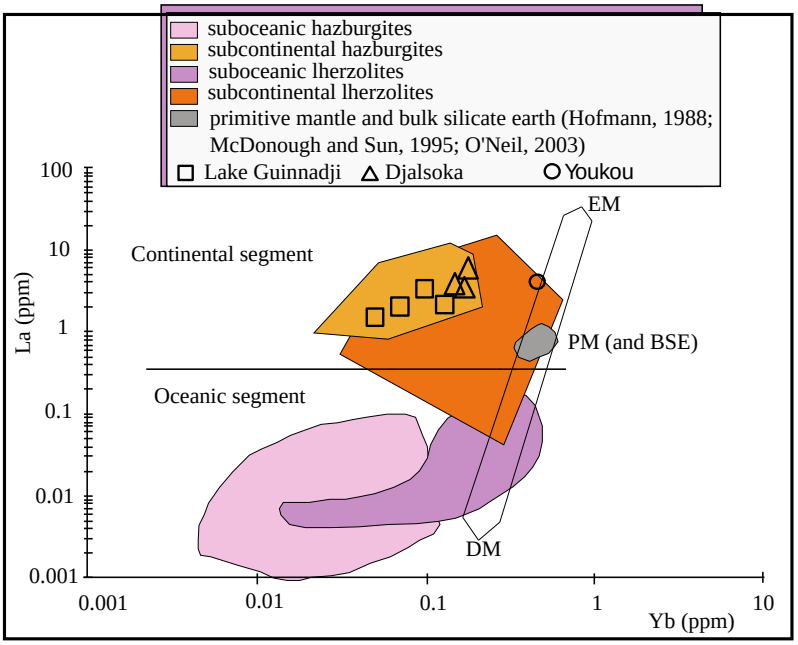

Fig 8

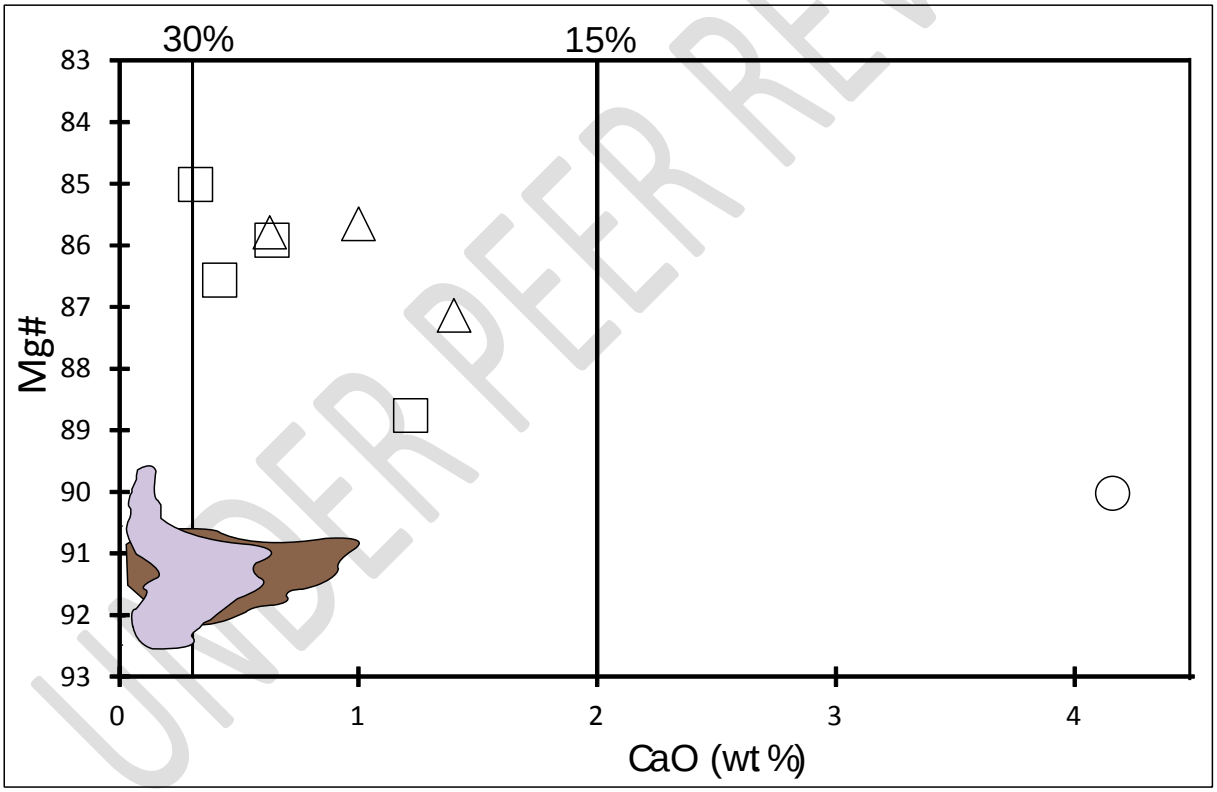

Fig 9

Table 1.

site	sample	coordinate

locality	sample	olivine	orthopyroxene	clinopyroxene	spinel	amphibole
Guinnadji	HD1	85	10	3	1	1
Guinnadji	HD2	78	15	6	1	0
Guinnadji	HD3	86	11	2	1	0
Guinnadji	HD5	76	17	4	2	1
Djalsoka	MO-03	82	11	5	1	1
Djalsoka	MO-10	74	15	8	2	1
Djalsoka	MO-12	81	12	5	1	1

Lake Guinnadji	HD1	N07°09’35’’ E13°44’32’’
Lake Guinnadji	HD2	N07°09’34’’ E13°44’34’’
Lake Guinnadji	HD3	N07°09’33’’ E13°44’35’’
Lake Guinnadji	HD5	N07°09’30’’ E13°44’33’’
Djalsoka volcano	MO-12	N07°10’35’’ E13°45’06’’
Djalsoka volcano	MO-03	N07°10’45’’ E13°45’23’’
Djalsoka volcano	MO-10	N07°10’45’’ E13°45’29’’

Table 2.

Table 3 :

locality	Guinnadji	Guinnadji	Guinnadji	Guinnadji	Djalsoka	Djalsoka	Djalsoka	Youkou
sample	HD1	HD2	HD3	HD5	MO-03	MO-10	MO-12	N-35
rock	harzburgite	harzburgite	harzburgite	harzburgite	harzburgite	harzburgite	harzburgite	lherzolite
SiO_2 (wt %)	40.84	43.60	40.59	41.10	41.40	42.10	43.60	42.81
TiO_2	0.07	0.14	0.06	0.15	0.15	0.21	0.18	0.04

Al_2O_3	0.62	1.54	0.66	0.71	0.67	1.23	1.45	2.05
Fe_2O_3	13.76	10.62	15.16	14.25	14.75	14.40	12.45	8.74
MnO	0.15	0.14	0.17	0.16	0.16	0.16	0.15	0.17
MgO	44.68	42.39	43.45	44.00	45.00	43.30	42.60	40.03
CaO	0.42	1.22	0.32	0.64	0.63	1.00	1.40	4.16
Na_2O	0.08	0.21	0.10	0.16	0.18	0.26	0.23	0.18
K_2O	0.05	0.10	0.08	0.09	0.08	0.13	0.09	0.02
P_2O_5	0.03	0.04	0.03	0.05	0.06	0.07	0.05	0.86
LOI	-1.10	-0.70	-1.00	-1.16	-1.21	-1.18	-1.00	0.23
sum	99.60	99.30	99.62	100.15	101.87	101.68	101.20	99.29
Mg#	86.57	88.77	85.02	85.92	85.79	85.65	87.14	90.03
CIPW norm								
Plagioclase	1.89	4.77	1.99	2.33	2.33	4.03	4.63	6.28
Orthoclase	0.30	0.59	0.47	0.53	0.47	0.77	0.53	0.12
Diopside	0.53	2.24	0.20	1.51	1.55	2.14	3.13	8.08
Hypersthene	12.09	21.21	13.25	11.35	9.40	11.94	18.54	16.32
Olivine	79.04	65.70	77.19	78.30	81.78	76.45	68.89	61.96
Ilmenite	0.13	0.27	0.11	0.28	0.28	0.40	0.34	0.08
Magnetite	6.64	5.12	7.32	6.89	7.12	6.96	6.00	4.20
Apatite	0.07	0.09	0.07	0.12	0.14	0.16	0.12	2.02
Be (ppm)	1	1	1					
Rb	0.8	1.8	1.6	2.1	2.5	4.3	2	
Sr	15.7	33.2	14.5	47.3	49.1	85.5	49.1	105
Cs	0.1	0.1	0.1	0.03	0.03	0.05	0.01	14.9
Ba	8	17	8	33.1	34.8	60.2	30.1	24
V	15	38	16	16	15	28	53	52
Cr_2O_3 (wt %)	0.057	0.313	0.028	0.042	0.032	0.071	0.177	0.2643
Co	146.7	119.2	168.9					114
Ni	2356	2309	2111					2408
Y	0.6	1.1	0.8	1.5	1.6	2.6	1.8	3
Zr	5.6	10.3	15.2	15	17	29	18	16
Hf	0.1	0.2	0.4	0.3	0.4	0.6	0.5	0.076
Nb	1.6	2.6	2.4	4.1	4.3	7.7	4.4	0.48
Ta	0.1	0.2	0.1	0.1	1	0.3	0.3	0.182
Th	0.1	0.2	0.3	0.41	0.46	0.74	0.4	0.27
U	0.1	0.1	0.1	0.15	0.28	0.22	0.12	0.101
La	1.5	2.2	2	3.3	3.9	6.2	3.6	2.46
Ce	2.1	4.4	3.6	6.7	7.6	12.2	7	4.85
Pr	0.18	0.51	0.34	0.73	0.85	1.46	0.83	0.45
Nd	1	2	1.3	3	3.2	5.4	3.2	1.51
Sm	0.07	0.32	0.13	0.62	0.61	1.23	0.53	0.193
Eu	0.05	0.12	0.06	0.17	0.15	0.27	0.22	0.083
Gd	0.2	0.26	0.15	0.35	0.54	0.93	0.42	0.29

Tb	0.03	0.05	0.02	0.06	0.05	0.12	0.06	
Dy	0.13	0.23	0.12	0.33	0.26	0.57	0.35	0.35
Ho	0.02	0.05	0.02	0.06	0.06	0.1	0.09	0.086
Er	0.07	0.15	0.07	0.12	0.15	0.22	0.21	0.24
Tm	0.01	0.01	0.01	0.02	0.02	0.03	0.03	
Yb	0.05	0.13	0.07	0.1	0.15	0.18	0.17	0.24
Lu	0.01	0.01	0.01	0.02	0.02	0.03	0.03	0.046
Ga	0.7	1.8	0.9	1.5	1.5	2.8	2.7	1
Sn	1	1	1	<1	<1	<1	<1	
Sc	7	9	7					14.9
W	0.5	0.5	0.6	<1	<1	<1	1	
Al_2O_3/MgO	0.01	0.04	0.02	0.02	0.01	0.03	0.03	0.05
Al_2O_3/TiO2	8.86	11.00	11.00	4.73	4.47	5.86	8.06	51.25
CaO/Al_2O_3	0.68	0.79	0.48	0.90	0.94	0.81	0.97	2.03
CaO/MgO	0.01	0.03	0.01	0.01	0.01	0.02	0.03	0.10
Na_2O/Al_2O_3	0.13	0.14	0.15	0.23	0.27	0.21	0.16	0.09
Na_2O/TiO_2	1.14	1.50	1.67	1.07	1.20	1.24	1.28	4.50
Ba/Rb	10.00	9.44	5.00	15.76	13.92	14.00	15.05	
Nb/Ta	16.00	13.00	24.00	41.00	4.30	25.67	14.67	2.64
Nb/Th	16.00	13.00	8.00	10.00	9.35	10.41	11.00	1.78
Sr/Nd	15.07	16.60	11.15	15.77	15.34	15.83	15.34	69.54
Y/Ho	30.00	22.00	40.00	25.00	26.67	26.00	20.00	34.88
Y/Nb	0.38	0.42	0.33	0.37	0.37	0.34	0.41	6.25
Zr/Hf	56.00	51.50	38.00	50.00	42.50	48.33	36.00	210.53
GdN/YbN	1.62	1.24	3.46	3.31	2.48	3.32	1.90	0.91
LaN/SmN	13.49	4.33	9.69	3.35	4.03	3.17	4.28	8.02
LaN/YbN	20.25	11.42	19.29	22.28	17.55	23.25	14.29	6.92
TbN/YbN	2.65	1.70	1.26	2.65	1.47	2.94	1.56	0.00